DOA Estimation in Distributed Nested Arrays Using Multifrequency Information Extrapolation

Zeqi Yang, Yiheng Liu, Hua Zhang, Yunpeng Wang, Jiawei Wang, and Xiaode Lyu, *Senior Member, IEEE*

***Abstract*—Distributed arrays can achieve an extended effective aperture through sparse spatial deployment, significantly enhancing the resolution of parameter estimation. However, the incomplete array aperture induced by long baselines between subarrays inevitably introduces angle ambiguity. To address this issue, this article proposes a distributed nested array interpolation method that leverages multifrequency information and low-rank matrix reconstruction for unambiguous direction-of-arrival (DOA) estimation. For distributed arrays with nested subarrays, the physical array is first mapped into the virtual array domain by vectorizing the covariance matrix. Subsequently, multifrequency measurements are incorporated to extrapolate the virtual array, effectively expanding the aperture of sparse distributed subarrays. To recover residual missing elements, a low-rank covariance matrix completion model is established, employing the Schatten-p norm to enforce low-rank constraints and incorporating sparsity priors within an optimization framework. The resulting problem is efficiently solved via an iteratively reweighted least squares (IRLSs) algorithm. Finally, the completed covariance matrix enables high-resolution DOA estimation through subspace-based techniques. Extensive simulation and field experimental results demonstrate the proposed method's effectiveness and robustness in achieving unambiguous, high-resolution DOA estimation in distributed array scenarios.**

***Index Terms*—Direction-of-arrival (DOA), distributed arrays, low-rank representation, multifrequency information, Schatten-p norm.**

I. Introduction

DISTRIBUTED coherent aperture radar has demonstrated significant potential in applications such as target detection, high-precision localization, and tracking, due to its capability of synthesizing an extended virtual aperture through spatially distributed subarrays [1]. Compared with conventional uniform arrays, distributed arrays achieve extended effective apertures through sparse subarray or element configurations while maintaining the same number of array elements. This configuration improves both the gain of the array and the accuracy of the angular estimation. Direction-of-arrival (DOA) estimation is one of the key research topics in distributed array signal processing and has significant application value in radar, sonar, wireless communication, and navigation systems [2], [3], [4]. Traditional DOA estimation methods are mainly based on centralized uniform arrays, and classical high-resolution subspace-based algorithms such as multiple signal classification (MUSIC) [5] and estimation of signal parameters via rotational invariance techniques (ESPRITs) [6] were originally designed under the assumption of uniform linear arrays (ULAs). Consequently, the degrees-of-freedom (DOF) and angular estimation performance are fundamentally constrained by the number of array elements. Increasing the number of elements can improve performance, but at the cost of higher hardware complexity and system expense. In contrast, distributed arrays offer flexible deployment strategies, enabling the realization of large-aperture array performance with relatively few nodes. This advantage makes them a compelling and efficient alternative, facilitating their widespread adoption in diverse practical applications [7], [8].

As a typical form of sparse array structure, distributed arrays exhibit significant spatial separation among their subarrays. While such long-baseline configurations can effectively extend the equivalent aperture and improve theoretical resolution, it inevitably introduces spatial discontinuity in received signals. Particularly in DOA estimation and signal reconstruction, where traditional algorithms are required to address the grating lobes and ambiguity problems inherent to distributed arrays. In [9], a virtual interpolated array transformation technique was proposed to fill the missing elements between subarrays with virtual elements, thereby converting the distributed array into a ULA with equal interelement spacing to suppress grating lobes. However, the computational complexity of such methods increases exponentially with the baseline length of the distributed array. Lee and Woo [10] addressed the angular ambiguity problem by employing interferometers with different configurations. Gazzah and Abed-Meraim [11] optimized the placement of subarrays using intelligent optimization algorithms to achieve an ambiguity-free optimal array configuration. However, these approaches substantially

Received 21 July 2025; revised 17 November 2025; accepted 15 December 2025. Date of publication 28 January 2026; date of current version 30 January 2026. The Associate Editor coordinating the review process was Dr. Takuma Watanabe. *(Corresponding author: Xiaode Lyu.)*

Zeqi Yang, Yiheng Liu, Hua Zhang, Yunpeng Wang, and Jiawei Wang are with the National Key Laboratory of Microwave Imaging, Aerospace Information Research Institute, Chinese Academy of Sciences, Beijing 100094, China, and also with the School of Electronic, Electrical and Communication Engineering, University of Chinese Academy of Sciences, Beijing 101499, China (e-mail: yangzeqi22@mails.ucas.ac.cn; liuyiheng17@mails.ucas.ac.cn; zhanghua211@mails.ucas.ac.cn; wangyunpeng23@mails.ucas.ac.cn; wangjiawei232@mails.ucas.ac.cn).

Xiaode Lyu is with the National Key Laboratory of Microwave Imaging, Aerospace Information Research Institute, Chinese Academy of Sciences, Beijing 100094, China (e-mail: lvxd@aircas.ac.cn).

Digital Object Identifier 10.1109/TIM.2026.3654749

increase the hardware cost and complexity of the radar system. Wong and Zoltowski [12] proposed the dual-size ESPRIT algorithm, which exploits two baseline scales in distributed arrays. This method derives an unambiguous coarse DOA estimate and an ambiguous fine estimate via ESPRIT, and then eliminates the phase ambiguity in the fine estimate by referencing the coarse estimate, resulting in an unambiguous and more accurate DOA estimate. However, such ambiguity-resolution techniques exhibit clear thresholds with respect to signal-to-noise ratio (SNR) and baseline length. When the SNR drops below critical thresholds or the baseline length exceeds optimal values, significant errors in coarse estimation may prevent successful ambiguity resolution, resulting in severe degradation of DOA estimation performance. Moreover, these methods do not increase the DOF of the array [13], [14]. Despite considerable progress in existing studies, the problems of aperture extension and DOA estimation for distributed arrays remain challenging. In particular, achieving high-accuracy signal reconstruction and unambiguous angle estimation in scenarios with low SNR and limited snapshots remains a significant challenge.

According to the spatial sampling theorem, the synthesized beampattern of the distributed array inevitably exhibits grating lobes, which can adversely affect target detection and parameter estimation. To address this issue, several studies have proposed representative sparse array configurations that achieve a large aperture while mitigating array ambiguity. The minimum-redundancy array and minimum-hole array presented in [15] and [16] can effectively increase the aperture; however, their element positions lack closed-form expressions, limiting their practicality in real-world applications. The nested array configuration, integrating both dense and sparse subarray spacings, was developed to mitigate this problem [17]. The difference co-array of the nested array is hole-free. Unlike the nested array, the coprime array is constructed from two sparse ULAs with element spacings that are coprime to each other, resulting in a larger interelement spacing than that of the nested array. This design increases the DOF and mitigates mutual coupling effects [18], [19]. However, the difference co-array of the coprime array typically contains holes, preventing direct application in parameter estimation. To address this limitation, an interpolation method combined with nuclear norm minimization (NNM) was developed [20] to map the coprime array onto a virtual ULA and reconstruct the Toeplitz matrix, thereby achieving high-accuracy DOA estimation even in underdetermined scenarios. In [21], a joint estimation method was introduced based on tensor parallel factor decomposition and atomic norm minimization (ANM), effectively achieving off-grid DOA estimation for bistatic multiple-input multiple-output radar under array failure conditions while avoiding the parameter pairing step required by traditional methods. Yadav and George [22] proposed truncated NNM to fill the holes in the difference co-array, thereby enhancing estimation accuracy. A Schatten-p norm-based low-rank matrix reconstruction model was introduced, with the optimization problem addressed through proximal alternating linearized minimization, thereby enhancing both estimation accuracy and computational efficiency [23]. The low-rank matrix completion theory provides an effective framework for handling missing elements or sparse sampling in arrays, allowing recovery of complete signal information. Furthermore, previous research has exploited the dependence of the array manifold on carrier frequency to design array structures with greater flexibility. A sparse ULA operating at two frequencies has been proposed to construct a virtual coprime array, which avoids the need for complex matrix completion algorithms and exploits multifrequency information to increase the DOF [24]. Guo et al. [25] analyzed the Cramér–Rao lower bound (CRB) of dual-frequency coprime arrays. In [26], a group sparsity-based interpolation method for multifrequency sparse arrays was developed to recover missing entries in the covariance matrix, achieving high-resolution DOA estimation. Zhang et al. [27] further utilized both the auto-correlation and cross-correlation information of multifrequency arrays, enabling reconstruction of a virtual ULA with expanded aperture suitable for distributed sensing scenarios. Park et al. [28] proposed an off-grid DOA estimation method based on atomic norm denoising, which can effectively handle multisnapshot and multifrequency data and achieve high-precision estimation in the presence of grid mismatch. Wen et al. [29] developed a multifrequency joint sparse Bayesian learning approach for passive radar DOA estimation, which exploits both frequency diversity and spatial sparsity to significantly enhance estimation accuracy and resolution under low SNR and limited snapshots. Wu et al. [30] proposed a multifrequency off-grid DOA estimation method based on ANM, which solves a semidefinite program and uses dual polynomial peak localization to address continuous parameter estimation in broadband scenarios. Guo and Dai [31] introduced a joint multiband DOA estimation algorithm based on low-rank matrix recovery, which constructs a unified frequency grid and applies proximal gradient descent to solve a nonconvex optimization problem, enabling high-accuracy estimation of overdetermined sources with few snapshots. Existing studies have demonstrated that multifrequency processing holds great potential for improving DOF and DOA estimation accuracy, as well as mitigating information loss caused by array holes or sparse sampling. Within the framework of distributed array systems, comprehensive studies on the coordinated utilization of multifrequency information to achieve aperture extension and resolve directional ambiguities are still limited. Overall, these methods primarily focus on the design of sparse arrays and the development of corresponding DOA estimation algorithms [32], [33].

To fully exploit the aperture extension capabilities of sparse subarrays and achieve unambiguous DOA estimation in distributed arrays, this article proposes a distributed nested array DOA estimation method based on multifrequency information extrapolation. By leveraging the additional DOF provided by multifrequency signals, the proposed method reconstructs an equivalent large-aperture array from distributed array measurements. Furthermore, it addresses the data missing problem caused by long baselines between subarrays by employing a multisubspace low-rank matrix representation model. The

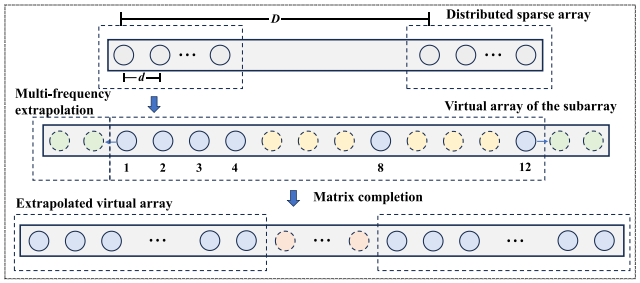

Fig. 1. Distributed nested array and the corresponding extrapolated virtual array.

array data is precisely reconstructed under Schatten-p norm regularization, enabling robust DOA estimation in distributed arrays.

In this article, we propose a distributed array DOA estimation framework that combines multifrequency information extrapolation and low-rank matrix completion techniques. The main contributions are as follows.

1) A distributed sensing architecture integrating multifrequency information is established, which fully exploits the virtual array of nested arrays to achieve higher DOF. This enables hole filling within subarrays as well as extrapolation across subarrays.
2) A low-rank matrix completion model for multifrequency distributed arrays is established, where the Schatten-p norm is employed to impose low-rank constraints, thus achieving a larger effective aperture. The model is solved using an iteratively reweighted least squares (IRLS) algorithm, which attains a larger array aperture and higher DOF compared to existing methods, while maintaining low computational complexity.
3) The relationship between the extrapolated virtual elements and the array structure is derived. The proposed algorithm can be extended to distributed arrays whose subarrays are arranged uniformly or randomly along a common line, without imposing specific constraints on subarray configurations.

The remaining part of this article is organized as follows. Section II establishes the received signal model for distributed nested arrays. In Section III, the array extrapolation method utilizing multifrequency information and the solution approach for the low-rank matrix completion model is derived. Section IV demonstrates the effectiveness of the method through both simulations and experimental results. Finally, Section V concludes this article.

Notation: In this article, bold lowercase and uppercase characters denote vectors and matrices, respectively. $(\cdot)^*$, $(\cdot)^T$, and $(\cdot)^H$ denote conjugate, transposition and conjugate transposition, respectively. vec$(\cdot)$ denotes the operation of vectorization. $\odot$ denotes Khatri–Rao product. $\otimes$ denotes the Kronecker product. $\|\cdot\|_{S_p}$ denotes the Schatten-p norm, $\|\cdot\|_{2,1}$ denotes the $l_{2,1}$ norm.

II. Signal Model

Consider a distributed system composed of L identical, collinearly placed subarrays, each configured as a two-level nested array. For each nested subarray, the inner ULA consists of N_1 elements with an interelement spacing of d_1, while the outer ULA consists of N_2 elements with an interelement spacing of $d_2 = (N_1 + 1)d_1$. To achieve the maximum DOF with a fixed total number of array elements, when the total number of elements is even, the virtual ULA is maximized by setting $N_1 = N_2$. Thus, the total number of physical elements in the distributed nested array is $N = 2LN_1$. Assume that the baseline length between adjacent subarrays is D, and that the array operates over a bandwidth that covers the desired frequency points. All subarrays can receive signals synchronously to enable coherent processing. Accordingly, the set of element positions in the distributed array can be expressed as

$$\mathbb{P} = \bigcup_{l=1}^{L} \mathbb{P}_l = \bigcup_{l=1}^{L} \{n\bar{d} + (l-1)D \cup n(N_1+1)\bar{d} + (l-1)D \mid 1 \le n \le N_1, 1 \le l \le L\} \tag{1}$$

where $\bar{d}$ denotes half-wavelength in a normalized frequency sense. For model simplification, we consider a distributed array consisting of two subarrays, as illustrated in Fig. 1. The proposed model, however, can be readily extended to configurations with multiple subarrays.

For I continuous wave signals with frequencies f_i $(i = 1, \ldots, I)$ impinging on the distributed arrays from K independent far-field narrowband targets, the corresponding received signal can be expressed as

$$\boldsymbol{x}_i(t) = e^{j2\pi f_i t} \sum_{k=1}^{K} \boldsymbol{s}_i^{(k)}(t)\, \boldsymbol{a}_i(\theta_k) + \boldsymbol{n}_i(t) \tag{2}$$

where $\boldsymbol{s}_i^{(k)}(t)$ denotes the reflection coefficient of the kth target at frequency f_i and $\boldsymbol{a}_i(\theta_k)$ is the steering vector, which can be expressed as

$$\boldsymbol{a}_i(\theta_k) = \left[1, \ldots, e^{-j\frac{2\pi N_1(N_1+1)d_i}{\lambda_i}\sin(\theta_k)}\right]^T \tag{3}$$

where $\lambda_i = c/f_i$ denotes the wavelength corresponding to the ith frequency. In addition, $\boldsymbol{n}_i(t) \sim \mathcal{CN}(0, \sigma_n^2 \mathbf{I}_{2N_1})$ represents additive white Gaussian noise.

After applying low-pass filtering, the received signal is further down-converted to baseband, resulting in

$$\begin{aligned}\boldsymbol{x}_i(t) &= \sum_{k=1}^{K} \boldsymbol{s}_i^{(k)}(t)\, \boldsymbol{a}_i(\theta_k) + \boldsymbol{n}_i(t) \\ &= \boldsymbol{A}_i \boldsymbol{S}_i(t) + \boldsymbol{N}_i(t)\end{aligned} \tag{4}$$

where $\boldsymbol{A}_i = [\boldsymbol{a}_i(\theta_1), \ldots, \boldsymbol{a}_i(\theta_K)]$ and $\boldsymbol{S}_i(t) = [\boldsymbol{s}_i^{(1)}(t), \ldots, \boldsymbol{s}_i^{(K)}(t)]^T$.

For a distributed array system consisting of two subarrays, the corresponding received signal vector is given by

$$\mathbf{x}(t) = \begin{bmatrix} \mathbf{A}_i \mathbf{S}_i(t) \\ \mathbf{A}_i \boldsymbol{\Phi} \mathbf{S}_i(t) \end{bmatrix} + \mathbf{N}_i(t) = \mathbf{A}\mathbf{S}(t) + \mathbf{N}(t) \tag{5}$$

where $\boldsymbol{\Phi} = \text{diag}\{e^{-j2\pi D\sin(\theta_1)/\lambda_i}, \ldots, e^{-j2\pi D\sin(\theta_K)/\lambda_i}\}$.

In this article, we synthesize a virtual single-frequency covariance matrix from multifrequency observations under the proportional spectrum assumption, i.e., $b_{i,j}^{(k)} = (s_i^k)/(s_j^k)$, $b_{i,j}^{(k)}$ is a constant, that the relative power ratios among different source signals remain constant across all operating frequencies. When the array operates at a reference frequency f_0, the received signal can be expressed as

$$\mathbf{x}(f_0) = \mathbf{A}(f_0)\mathbf{S}(f_0) + \mathbf{N}(f_0). \tag{6}$$

Assuming the incident signals are uncorrelated, the received signal covariance matrix at frequency f_0 is given by

$$\begin{aligned}\hat{\mathbf{R}}_{\boldsymbol{x}}(f_0) &= E\left\{\mathbf{x}(f_0)\mathbf{x}^H(f_0)\right\} \\ &= \mathbf{A}(f_0)\mathbf{p}(f_0)\mathbf{A}^H(f_0) + \sigma_n^2(f_0)\mathbf{I}_{2N_1}\end{aligned} \tag{7}$$

where $\mathbf{p}(f_0) = \mathrm{diag}\{\sigma_1^2(f_0), \ldots, \sigma_K^2(f_0)\}$, and $\sigma_k^2(f_0)$ represents the power of the kth signal at frequency f_0. By vectorizing the covariance matrix of the received signal, we obtain

$$\mathbf{z}(f_0) = \mathrm{vec}\left(\hat{\mathbf{R}}_{\boldsymbol{x}}(f_0)\right) = \tilde{\mathbf{A}}(f_0)\mathbf{p}(f_0) + \sigma_n^2(f_0)\tilde{\mathbf{i}} \tag{8}$$

where $\tilde{\mathbf{A}}(f_0) = \mathbf{A}^*(f_0) \odot \mathbf{A}(f_0)$, $\tilde{\mathbf{i}} = \mathrm{vec}(\mathbf{I}_{2N_1})$. For the received signals at the operating frequency, vectorizing the covariance matrix forms a virtual array, whose virtual element positions are determined by the original array geometry and the signal frequency. Selecting frequency points f_q, the received signal at frequency $f_q = \alpha_q f_0$ can be expressed as

$$\mathbf{x}(f_q) = \mathbf{A}(f_q)\mathbf{S}(f_q) + \mathbf{N}(f_q). \tag{9}$$

Then, the vectorized covariance matrix of the received signal at frequency f_q is given by

$$\mathbf{z}(f_q) = \mathrm{vec}\left(\hat{\mathbf{R}}_{\boldsymbol{x}}(f_q)\right) = \tilde{\mathbf{A}}(f_q)\mathbf{p}(f_q) + \sigma_n^2(f_q)\tilde{\mathbf{i}} \tag{10}$$

where $\tilde{\mathbf{A}}(f_q) = \mathbf{A}^*(f_q) \odot \mathbf{A}(f_q)$. The positions of the virtual array elements, formed by the covariance matrices at different frequencies, are closely related to the ratio between the frequency f_q and the operating frequency f_0. This relationship can be interpreted as scaling the original virtual array element positions by a factor of α_q. Thus, the virtual array at frequency f_q can be viewed as a proportionally scaled version of the virtual array at the operating frequency f_0. In particular, when $f_q > f_0$, the array is effectively expanded, whereas when $f_q < f_0$, the array is proportionally compressed.

III. Proposed Method

A. Virtual Array Extrapolation Using Multifrequency Information

In distributed arrays, frequency diversity can be effectively exploited to extend the equivalent aperture of the array, thereby enhancing resolution and estimation accuracy. For subarrays operating at identical frequencies, virtual array extrapolation can be accomplished by either leveraging the inherent multifrequency components available within the system bandwidth or actively transmitting specially designed narrowband signals with varied carrier frequencies to synthesize the required frequency diversity. This enables extrapolation of the subarrays to fill partial holes caused by long baselines, thereby enhancing the equivalent aperture of the array and improving spatial resolution.

The support matrix of the array can intuitively represent the position of each element of the vectorized covariance matrix at different frequencies within the virtual array. For the array received signal at the operating frequency f_0, the steering matrix can be expressed as

$$\left[\mathbf{A}(f_0)\right]_{i,k} = e^{-j2\pi f_0 x_i \sin(\theta_k)/c}.$$

The phase difference of the (i, j)th element in the array covariance matrix is given by $e^{-j2\pi f_0(x_i - x_j)\sin(\theta_k)/c}$. When sampling at multiple frequencies f_q, it is equivalent to obtaining observations at different spatial scales in the space domain. For a given frequency f_q, we have

$$e^{-j2\pi f_q(x_i - x_j)\sin(\theta_k)/c} = e^{-j2\pi f_0 \alpha_q(x_i - x_j)\sin(\theta_k)/c}. \tag{11}$$

Thus, the variation in frequency is equivalent to a spatial scaling of the element positions, enabling the use of multifrequency information to fill the spatial gaps caused by long baselines in distributed arrays.

To intuitively reflect the positions of virtual elements after vectorizing the covariance matrix, the self-lag set is defined as the set of virtual element positions obtained from the same frequency, i.e.,

$$\begin{aligned}\mathbb{C}_{\mathrm{self}} &= \bigcup_{l=1}^{L} \mathbb{P}_l \ominus \mathbb{P}_l \\ &= \left\{x_i - x_j \mid i, j = 1, \ldots, N\right\}\end{aligned} \tag{12}$$

where $\ominus$ denotes the lag between two sets. x_i and x_j represent the positions of the ith and jth elements of the distributed array relative to the array reference point. The (i, j)th entry of the support matrix $[\boldsymbol{C}(f_0)]_{i,j}$ is derived from the set $\mathbb{C}_{\mathrm{self}}$. For the received signal at frequency f_q, the corresponding set of virtual element positions can be expressed as $\mathbb{C}(f_q) = \{\alpha_q x_i - \alpha_q x_j \mid i, j = 1, \ldots, N\}$.

Accordingly, the (i, j)th entry of the support matrix $[\boldsymbol{C}(f_q)]_{i,j}$ is associated with the set $\mathbb{C}(f_q)$. Based on this definition, the union of the virtual element position sets obtained at multiple frequencies is given by

$$\begin{aligned}\mathbb{C}_{\mathrm{multi}} &= \bigcup_{q=1}^{Q} \mathbb{C}(f_q) \\ &= \bigcup_{q=1}^{Q} \left\{\alpha_q x_i - \alpha_q x_j \mid i, j = 1, \ldots, N\right\}.\end{aligned} \tag{13}$$

For a single subarray, the continuous virtual array element distribution spans from $-N_1^2 - N_1 + 1$ to $N_1^2 + N_1 - 1$, with DOF given by $2N_1(N_1 + 1) - 1$.

For the virtual array of nested subarrays, multifrequency information can be exploited to extrapolate and fill in some of the holes caused by long baselines, thereby enhancing the effective aperture of the array. In particular, we consider a distributed array composed of two-level nested subarrays, $N_1 = N_2 = 3$. The unit element spacing d_0 of each subarray corresponds to half the wavelength at the operating frequency. The baseline length of the distributed array is 28 times the unit element spacing, i.e., $D = 28$. Taking the first element as the reference point of the array, the element positions

of the subarrays are given by $[1d_0, 2d_0, 3d_0, 4d_0, 8d_0, 12d_0]$ and $[29d_0, 30d_0, 31d_0, 32d_0, 36d_0, 40d_0]$, respectively. As an example, for the first subarray, the support matrix at the operating frequency f_0 is expressed as

$$\mathbf{C}(f_0) = \begin{bmatrix} 0 & -1 & -2 & -3 & -7 & -11 \\ 1 & 0 & -1 & -2 & -6 & -10 \\ 2 & 1 & 0 & -1 & -5 & -9 \\ 3 & 2 & 1 & 0 & -4 & -8 \\ 7 & 6 & 5 & 4 & 0 & -4 \\ 11 & 10 & 9 & 8 & 4 & 0 \end{bmatrix}. \tag{14}$$

It can be seen that the virtual array of the nested subarray has a continuous element distribution ranging from $-11d_0$ to $11d_0$. To further extrapolate the array using multifrequency information, it is necessary to select appropriate frequency points either within the bandwidth covered by the signal or from narrowband signals at different frequencies. The relative bandwidth of the signal is related to its center frequency

$$\eta = \frac{B}{f_c} \tag{15}$$

where, B denotes the signal bandwidth, and f_c is the center frequency of the signal. For the same bandwidth, a higher center frequency results in a smaller relative bandwidth, whereas a lower center frequency leads to a larger relative bandwidth. Suppose we intend to exploit multifrequency information to extrapolate additional elements, for the above array, if we aim to add a virtual element at position $12d_0$, it becomes necessary to introduce an additional frequency $f_1 = 12/11 f_0$. In this case, the support matrix becomes

$$\mathbf{C}(f_1) = \begin{bmatrix} 0 & -\frac{12}{11} & -\frac{24}{11} & -\frac{36}{11} & -\frac{84}{11} & -12 \\ \frac{12}{11} & 0 & -\frac{12}{11} & -\frac{24}{11} & -\frac{72}{11} & -\frac{120}{11} \\ \frac{24}{11} & \frac{12}{11} & 0 & -\frac{12}{11} & -\frac{60}{11} & -\frac{108}{11} \\ \frac{36}{11} & \frac{24}{11} & \frac{12}{11} & 0 & -\frac{48}{11} & -\frac{96}{11} \\ \frac{84}{11} & \frac{72}{11} & \frac{60}{11} & \frac{48}{11} & 0 & -\frac{48}{11} \\ 12 & \frac{120}{11} & \frac{108}{11} & \frac{96}{11} & \frac{48}{11} & 0 \end{bmatrix}.$$

It can be observed that by leveraging multifrequency information, a virtual element is obtained at position $12d_0$, thereby extending the array aperture and increasing the DOF.

To reduce hardware costs, it is sufficient to use only a subset of the array elements to fill in the missing positions. For example, the elements located within $[1, 12]d_0$ can be used to receive the signal at frequency f_1. The corresponding entries in the support matrix at frequency f_1 for these two elements are then given by

$$\mathbf{C}(f_1) = \frac{12}{11} C(f_0) = \frac{12}{11} \begin{bmatrix} 0 & -11 \\ 11 & 0 \end{bmatrix} d_0 = \begin{bmatrix} 0 & -12 \\ 12 & 0 \end{bmatrix} d_0.$$

To select appropriate frequency points, the additional frequencies required for extrapolation should fall within the signal's bandwidth range or within the desired narrowband signal frequencies receivable by the array. For the distributed nested array configuration shown in Fig. 1 in the manuscript, after vectorizing the covariance matrix and removing redundant terms, the virtual steering vector of the virtual array at frequency f_0 can be expressed as

$$a_v(f_0) = \left[e^{-j2\pi D \sin(\theta_k)/\lambda}, 1, e^{j2\pi D \sin\theta_k/\lambda}\right]^T \otimes \bar{a}(\theta_k). \tag{16}$$

where

$$\bar{a}(\theta_k) = \left[e^{-j2\pi\left(N_1^2+N_1-1\right)d_0 \sin(\theta_k)/\lambda}, \ldots, 1, \ldots, e^{j2\pi\left(N_1^2+N_1-1\right)d_0 \sin(\theta_k)/\lambda}\right]^T. \tag{17}$$

Due to the inherent symmetry of the virtual array, the virtual elements located on the positive half-axis are considered. From the steering vector formulation, it can be observed that the missing entries in the vectorized covariance matrix correspond to the virtual array within $N_1^2 + N_1 \sim D - (N_1^2 + N_1)$. To compensate for these missing elements, additional frequency points are required, and the number of necessary frequencies can be estimated as $D - 2(N_1^2 + N_1) + 1$.

Assuming that the system hardware permits extrapolation within a limited bandwidth, the number of usable frequency points is denoted as Q. Based on the above analysis, the additional frequency selection criteria are as follows: $f_q = (Q + N_1^2 + N_1 - 1)/(N_1^2 + N_1 - 1) f_0$, $f_q = (D - (Q + N_1^2 + N_1 - 1))/(D - (N_1^2 + N_1 - 1)) f_0$, and within the available bandwidth, the following conditions should be satisfied:

$$\frac{2 \times \left|f_q - f_0\right|}{f_0} \le \eta. \tag{18}$$

That is: $\eta \ge 2Q/M$, let

$$M = \max\left(N_1^2 + N_1 - 1, D - N_1^2 - N_1 + 1\right).$$

The validity of this formulation relies on the following assumptions.

1) *Bandwidth Matching Condition:* The chosen frequency points should fall within the system's available bandwidth, or within the narrowband range receivable by the receiver.
2) *Proportional Spectrum Assumption:* The multifrequency extrapolation is based on the proportional spectrum assumption, which requires that the normalized source powers maintain constant relative ratios across all operating frequencies. This condition implies that the scattering responses of different targets do not introduce frequency-dependent variations that would alter their relative power levels. Under this assumption, the array responses at different frequencies can be consistently mapped to a common virtual spatial domain through appropriate scaling.
3) *Angle Consistency Condition:* Multifrequency components originating from the same physical source should have identical DOA.

When these conditions are satisfied, the spatial mapping model for multifrequency information is valid, enabling effective aperture extension and continuous filling in the virtual array domain.

Based on the above analysis, multifrequency information can be used to extrapolate Q additional virtual elements for

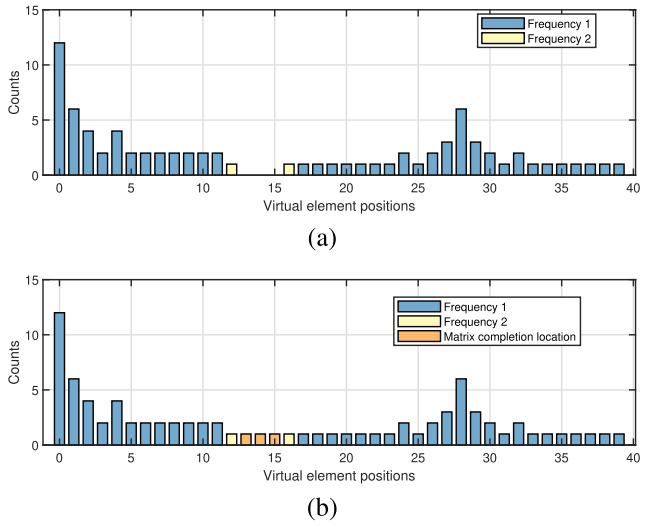

Fig. 2. Position of virtual array elements in distributed array. (a) Extrapolating with multifrequency information. (b) Complementing the array aperture with a low-rank matrix.

each of the two subarrays, thereby filling in the missing positions caused by the long baseline of the distributed array. The positions of the virtual array elements on the positive half-axis after aperture extrapolation are shown in Fig. 2.

Since the radar cross section of the target varies with frequency, the received signals cannot be directly concatenated and processed for array aperture extension. Assuming the target signal is stationary, its energy, i.e., the second-order moment, remains constant. Therefore, by vectorizing the covariance matrices, the virtual array data constructed from multiple frequencies can be concatenated to complement the data at the operating frequency. However, as the signal power and noise power may vary across different frequencies, it is necessary to normalize the covariance matrices at both the operating frequency and the complementary frequencies before constructing a unified virtual array. The normalized covariance matrix can be expressed as

$$\left[\mathbf{R}_{\boldsymbol{x}}\left(f_q\right)\right]_{i,j}=\frac{E\left\{\left[\boldsymbol{x}\left(f_q\right)\right]_i\left[\boldsymbol{x}^*\left(f_q\right)\right]_j\right\}}{\frac{1}{N_s(f_q)}E\left\{\mathbf{x}^H\left(f_q\right)\mathbf{x}\left(f_q\right)\right\}} \tag{19}$$

where $[\mathbf{R}_{\boldsymbol{x}}(f_q)]_{i,j}$ denotes the (i, j)th element of the normalized covariance matrix $\mathbf{R}_x(f_q)$, $N_s(f_q)$ is the number of array elements operating at frequency f_q, and $[\boldsymbol{x}(f_q)]_i$ represents the signal received by the ith array element at frequency f_q. The normalized signal power and noise power can be expressed as

$$\bar{\sigma}_k^2\left(f_q\right)=\frac{\sigma_k^2\left(f_q\right)}{\sum_{k=1}^{K}\sigma_k^2\left(f_q\right)+\sigma_n^2\left(f_q\right)} \tag{20}$$

$$\bar{\sigma}_n^2\left(f_q\right)=\frac{\sigma_n^2\left(f_q\right)}{\sum_{k=1}^{K}\sigma_k^2\left(f_q\right)+\sigma_n^2\left(f_q\right)} \tag{21}$$

where $\bar{\sigma}_k^2(f_q)$ denotes the normalized signal power, and $\bar{\sigma}_n^2(f_q)$ denotes the normalized noise power. This normalization ensures that, under the same SNR conditions, the construction of the virtual array is not affected by the variations in signal power across different frequencies.

In practical systems, the selection of multifrequency extrapolation parameters should take into account the signal bandwidth, the system's tunable frequency range, and the desired aperture extension capability. The number of extrapolated frequency points Q is primarily constrained by the hardware capabilities and the available bandwidth of the system. Furthermore, each frequency point should include at least 100 snapshots to ensure stable covariance estimation. It should be noted that although the above analysis focuses on distributed nested arrays, the proposed method can be readily extended to other subarray configurations.

B. Low-Rank Matrix Completion Model

Due to practical hardware constraints, it is challenging to fully compensate for the large baseline gaps inherent in distributed arrays solely by extrapolating with multifrequency information from the subarrays. To further enhance the accuracy and robustness of aperture completion, it is necessary to leverage the low-rank structure inherent in the received signal to reconstruct the covariance matrix. In particular, the virtual array is treated as single-snapshot measurement data, for which the covariance matrix theoretically exhibits rank one. We employ a Toeplitz matrix reconstruction approach. After partially filling in the missing elements using multifrequency extrapolation, zeros are inserted into the remaining missing positions to construct a virtual continuous ULA $\mathbf{z}_{\mathbb{V}}$. Exploiting the Hermitian symmetry of $\mathbf{z}_{\mathbb{V}}$, an extended Hermitian Toeplitz matrix is then formulated to represent the enlarged effective aperture, where $\mathbf{z}_{\mathbb{V}}$ denotes the virtual observation vector derived by removing redundant elements and averaging the measurements corresponding to identical virtual element positions

$$\mathbf{X}_{\mathbb{V}}=\begin{bmatrix}[\mathbf{z}_{\mathbb{V}}]_P & [\mathbf{z}_{\mathbb{V}}]_{P-1} & \cdots & [\mathbf{z}_{\mathbb{V}}]_1\\ [\mathbf{z}_{\mathbb{V}}]_{P+1} & [\mathbf{z}_{\mathbb{V}}]_P & \cdots & [\mathbf{z}_{\mathbb{V}}]_2\\ \vdots & \vdots & \ddots & \vdots\\ [\mathbf{z}_{\mathbb{V}}]_{2P-1} & [\mathbf{z}_{\mathbb{V}}]_{2P-2} & \cdots & [\mathbf{z}_{\mathbb{V}}]_P\end{bmatrix}. \tag{22}$$

The obtained covariance matrix $\mathbf{X}_{\mathbb{V}}$ is formed by concatenating signal data collected at multiple frequencies. Each frequency component can be interpreted as the signal received by array elements located at different positions, where the corresponding covariance matrices represent samples drawn from multiple signal subspaces under the assumption of sparse noise.

In this article, we formulate the covariance matrix $\mathbf{X}_{\mathbb{V}}$ of the distributed virtual array as a linear combination of dictionary atoms under a low-rank representation model, where the coefficient matrix is constrained to be low-rank. To promote this low-rank structure, we adopt the Schatten-p norm with $0 < p < 1$ as the regularization term.

Prior studies have shown that, compared to the nuclear norm, the Schatten-p norm provides a closer approximation to the rank function and thus achieves a more accurate

characterization of the matrix rank minimization problem. The optimization problem can be formulated as

$$\min_{\mathbf{Z},\mathbf{E}} \ \|\mathbf{Z}\|_{S_p}^p + \lambda\|\mathbf{E}\|_{2,1} \quad \text{s.t. } \mathbf{X}_{\mathbb{V}} = \mathbf{X}_{\mathbb{V}}\mathbf{Z} + \mathbf{E}. \tag{23}$$

The problem can be reformulated as

$$\min_{\mathbf{Z}\in\mathbb{R}^{P\times P}} J(\mathbf{Z}) = \|\mathbf{Z}\|_{S_p}^p + \lambda\|\mathbf{X}_{\mathbb{V}}\mathbf{Z} - \mathbf{X}_{\mathbb{V}}\|_{2,1} \tag{24}$$

where $\|\mathbf{X}\|_{S_p}^p = \sum_{i=1}\sigma_i^p(\mathbf{X})$ denotes the Schatten-p norm, and $\|\mathbf{X}\|_{2,1} = \sum_j \|\mathbf{X}_j\|_2$ denotes the $l_{2,1}$ norm, which is used to enforce sparsity in the noise component. In practice, since $\|\mathbf{X}\|_{S_p}^p = \mathrm{Tr}((\mathbf{X}^T\mathbf{X})^{p/2})$, both terms in the objective function are nonsmooth. According to [34], an additional regularization term can be introduced to smooth these terms

$$\min_{\mathbf{Z}} J(\mathbf{Z},\mu) = \left\|\begin{bmatrix}\mathbf{Z}\\ \mu\mathbf{I}\end{bmatrix}\right\|_{S_p}^p + \lambda\left\|\begin{bmatrix}\mathbf{X}_{\mathbb{V}}\mathbf{Z} - X_{\mathbb{V}}\\ \mu\mathbf{1}^T\end{bmatrix}\right\|_{2,1} \tag{25}$$

where $\mu > 0, \mathbf{I} \in \mathbb{R}^{P\times P}$ denotes the identity matrix, and $\mathbf{1} \in \mathbb{R}^P$ represents an all-ones vector. The above equation can be further rewritten as

$$\min_{\mathbf{Z}} \mathrm{Tr}\left(\mathbf{Z}^T\mathbf{Z} + \mu^2\mathbf{I}\right)^{\frac{p}{2}} + \lambda\sum_{i=1}^{P}\left(\|(\mathbf{X}_{\mathbb{V}}\mathbf{Z} - \mathbf{X}_{\mathbb{V}})_i\|_2^2 + \mu^2\right)^{1/2}$$

where $(\mathbf{X})_i$ denotes the ith column of matrix $\mathbf{X}$.

Let $L(\mathbf{Z}) = \mathrm{Tr}(\mathbf{Z}^T\mathbf{Z} + \mu^2\mathbf{I})^{p/2}, S(\mathbf{Z}) = \sum_{i=1}^{P}\left(\|(\mathbf{X}_{\mathbb{V}}\mathbf{Z} - X_{\mathbb{V}})_i\|_2^2 + \mu^2\right)^{1/2}$

$$J(\mathbf{Z},\mu) = L(\mathbf{Z}) + \lambda S(\mathbf{Z}). \tag{26}$$

Taking the derivative of $L(\mathbf{Z})$

$$\frac{\partial L}{\partial \mathbf{Z}} = p\mathbf{Z}\left(\mathbf{Z}^T\mathbf{Z} + \mu^2\mathbf{I}\right)^{p/2-1} = p\mathbf{Z}\mathbf{U} \tag{27}$$

let $\mathbf{U} = (\mathbf{Z}^T\mathbf{Z} + \mu^2\mathbf{I})^{p/2-1}$.

Define $\mathbf{U}$ as the weight matrix associated with $L(\mathbf{Z})$. This makes it possible to determine $\mathbf{U}$ without the need for explicit singular value decomposition.

We take the derivative of each column of $S(\mathbf{Z})$ individually

$$\begin{aligned}\frac{\partial S}{\partial \mathbf{Z}_i} &= \frac{2\mathbf{X}_{\mathbb{V}}^T(\mathbf{X}_{\mathbb{V}}\mathbf{Z} - \mathbf{X}_{\mathbb{V}})_i}{2\left(\|(\mathbf{X}_{\mathbb{V}}\mathbf{Z} - \mathbf{X}_{\mathbb{V}})_i\|_2^2 + \mu^2\right)^{1/2}}\\ &= \frac{\mathbf{X}_{\mathbb{V}}^T\mathbf{X}_{\mathbb{V}}\mathbf{Z}_i - \mathbf{X}_{\mathbb{V}}^T(\mathbf{X}_{\mathbb{V}})_i}{\left(\|(\mathbf{X}_{\mathbb{V}}\mathbf{Z} - \mathbf{X}_{\mathbb{V}})_i\|_2^2 + \mu^2\right)^{1/2}}\\ &= \mathbf{X}_{\mathbb{V}}^T(\mathbf{X}_{\mathbb{V}}\mathbf{Z} - X_{\mathbb{V}})\mathbf{V}.\end{aligned} \tag{28}$$

Define $\mathbf{V}$ as the weight matrix corresponding to $S(\mathbf{Z})$

$$V_{ii} = \left(\|(\mathbf{X}_{\mathbb{V}}\mathbf{Z} - \mathbf{X}_{\mathbb{V}})_i\|_2^2 + \mu^2\right)^{-1/2}. \tag{29}$$

Let $(\partial J)/(\partial \mathbf{Z}) = 0$, and $(\partial J)/(\partial \mathbf{Z}) = p\mathbf{Z}\mathbf{U} + \lambda\mathbf{X}_{\mathbb{V}}^T(\mathbf{X}_{\mathbb{V}}\mathbf{Z} - \mathbf{X}_{\mathbb{V}})\mathbf{V} = 0$.

Expanding the above equation, we have

$$p\mathbf{Z}\mathbf{U} + \lambda\mathbf{X}_{\mathbb{V}}^T\mathbf{X}_{\mathbb{V}}\mathbf{Z}\mathbf{V} - \lambda\mathbf{X}_{\mathbb{V}}^T\mathbf{X}_{\mathbb{V}}\mathbf{V} = 0. \tag{30}$$

Gathering all terms containing $\mathbf{Z}$ on the left-hand side and moving the constant terms to the right-hand side gives

$$p\mathbf{Z}\mathbf{U} + \lambda\mathbf{X}_{\mathbb{V}}^T\mathbf{X}_{\mathbb{V}}\mathbf{Z}\mathbf{V} = \lambda\mathbf{X}_{\mathbb{V}}^T\mathbf{X}_{\mathbb{V}}\mathbf{V}. \tag{31}$$

Multiplying both sides by $\mathbf{V}^{-1}$, we further obtain

$$\lambda\mathbf{X}_{\mathbb{V}}^T\mathbf{X}_{\mathbb{V}}\mathbf{Z} + p\mathbf{Z}\left(\mathbf{U}\mathbf{V}^{-1}\right) = \lambda\mathbf{X}_{\mathbb{V}}^T\mathbf{X}_{\mathbb{V}}. \tag{32}$$

Algorithm 1 Unambiguous DOA Estimation Algorithm for Distributed Arrays

Require: Received signals $\mathbf{x}(t)$
Ensure: DOAs θ_k

1: Estimate the covariance matrix $\mathbf{R_x}$ from the received signals of each distributed subarray;
2: Compute the covariance matrices of the array received data at the supplementary frequencies f_i.
3: Unified to the virtual array element position, and extrapolated the array by using multifrequency information;
4: Obtain the received signals of the co-array, and construct a Toeplitz matrix $\mathbf{X}_{\mathbb{V}}$;
5: Establish the matrix completion model according to (23);
6: Initialize $\mathbf{Z} = 0,\ t = 0,\ \mathbf{U}_t = \mathbf{V}_t = \mathbf{I} \in \mathbb{R}^{P\times P},\ \mu > 0,\ \alpha > 0,\ \lambda > 0,\ \varepsilon > 0$, maximum number of iterations $N_{\max}$;
7: **for** $k = 1$ *to* $N_{\max}$ **do**
8: Update $\mathbf{Z}$ by Equation (32);
9: Update $\mathbf{U}, \mathbf{V}$ by

$$\mathbf{U}_{t+1} = \left(\mathbf{Z}_{t+1}^T\mathbf{Z}_{t+1} + \mu^2\mathbf{I}\right)^{-1/2}$$

$$\left(\mathbf{V}_{t+1}\right)_{i,j} = \begin{cases}\left(\|(\mathbf{X}_{\mathbb{V}}\mathbf{Z} - \mathbf{X}_{\mathbb{V}})_i\|_2^2 + \mu^2\right)^{-1/2} & i = j\\ 0 & i \neq j\end{cases}$$

10: $t = t + 1,\ \mu = \mu/\alpha$;
11: Converged or $\|\mathbf{Z}_{t+1} - \mathbf{Z}_t\|_\infty \le \varepsilon$;
12: **end for**
13: Obtain $\mathbf{X}$ and perform MUSIC to estimate the DOAs θ_k.

This is a standard Sylvester equation of the form $\mathbf{A}\mathbf{Z} + \mathbf{Z}\mathbf{B} = \mathbf{C}$, where $\mathbf{A} = \lambda\mathbf{X}_{\mathbb{V}}^T\mathbf{X}_{\mathbb{V}}, \mathbf{B} = p\mathbf{U}\mathbf{V}^{-1}, \mathbf{C} = \lambda\mathbf{X}_{\mathbb{V}}^T\mathbf{X}_{\mathbb{V}}$, which can be efficiently solved in MATLAB using the lyap function. Finally, the solution $\mathbf{X} = \mathbf{X}_{\mathbb{V}}\mathbf{Z}$ yields the low-rank representation of the signal, which can subsequently be applied to subspace-based DOA estimation algorithms. The proposed algorithm is described in Algorithm. 1.

IV. Experimental Results

In this section, we verify the effectiveness of the proposed algorithm through simulation and experimental results. We consider a distributed array consisting of two identical nested subarrays, as illustrated in Fig. 1, $N_1 = N_2 = 3$, with a total of 12 elements. The baseline length between the two subarrays is $D = 28$. The parameters for the low-rank matrix completion are $p = 0.5,\ \lambda = 0.1,\ \alpha = 1.1,\ \varepsilon = 10^{-4},\ \mu_0 = 0.1\|\mathbf{X}_{\mathbb{V}}\|_2$, and the maximum number of iterations is $N_{\max} = 500$. We first evaluate the advantage of the proposed method in extending the effective aperture of the distributed array. Subsequently, we compare its performance with several representative algorithms, including the DOA estimation method based on the NNM method, the ANM method, the dual-size ESPRIT algorithm, and the conventional MUSIC algorithm and Capon algorithm without array interpolation. All signals are assumed

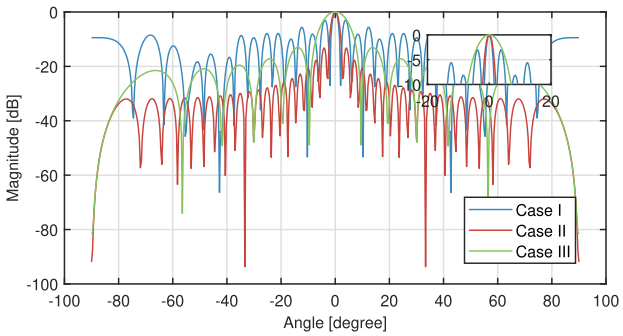

Fig. 3. Pattern of different array configurations with the same number of elements.

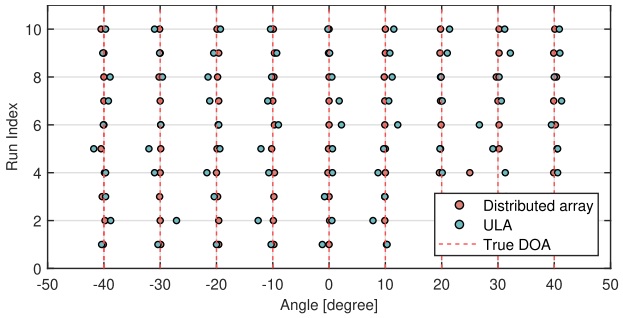

Fig. 4. DOA estimation performance of distributed array and ULA.

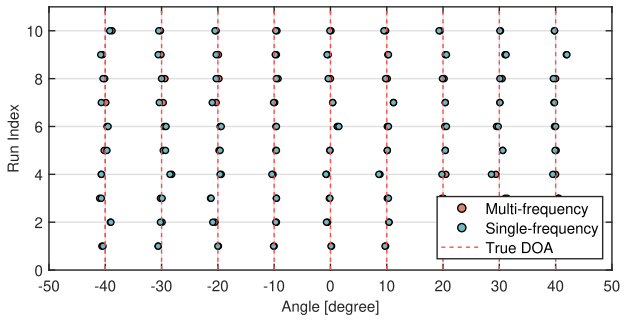

Fig. 5. DOA estimation performance of multifrequency and single-frequency arrays.

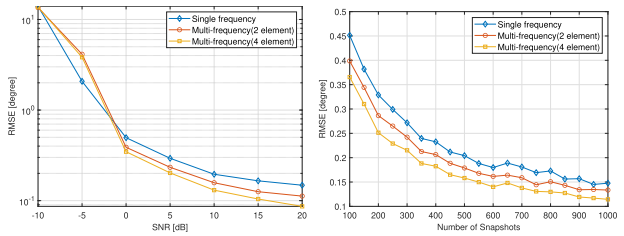

Fig. 6. Curve of DOA estimation performance of multifrequency and single-frequency arrays. (a) RMSEs of estimated DOAs versus SNR. (b) RMSEs of estimated DOAs versus snapshot numbers.

to be uncorrelated with each other. The root mean square error (RMSE) is used as the performance metric.

A. Aperture Extension Performance of Distributed Arrays

We first demonstrate the aperture extension capability of the distributed array. In particular, we consider three array configurations, each with the same total number of 12 elements: 1) a distributed nested array without aperture completion; 2) a distributed nested array after aperture completion; and 3) a ULA. The corresponding beam patterns for these configurations are shown in Fig. 3. Compared with the ULA under the same number of elements, the distributed array achieves a larger effective aperture, resulting in a narrower mainlobe width. However, the distributed array without aperture completion exhibits relatively higher sidelobe levels. By applying aperture completion, the distributed array can effectively enhance its equivalent aperture, thereby significantly improving its angle estimation performance.

We consider nine targets uniformly distributed over the angular range of -40° to 40°, which illuminate both the proposed distributed array configuration and a ULA with identical element count. Each algorithm undergoes ten independent estimation trials, with the comparative results presented in Fig. 4. The proposed method effectively fills the missing virtual element positions in the distributed array by integrating multifrequency information and performing matrix completion. This significantly extends the equivalent aperture of the array, leading to higher accuracy in DOA estimation. In contrast, conventional ULA suffers from limited aperture, resulting in notably lower estimation accuracy compared to the proposed method.

B. Subarray Aperture Extension Using Multifrequency Information

This section validates the effectiveness of aperture extension using multifrequency information through simulation experiments. For the single-subarray scenario, two array configurations are considered: one consisting of a single-frequency ULA without multifrequency exploitation, and the other featuring an extended aperture achieved through the fusion of multifrequency information. In particular, a ULA with $N = 12$ elements is considered, with the SNR set to 0 dB and the number of snapshots set to 200. Targets are uniformly distributed within the angular range of -40° to 40°. Two additional frequency points are selected to extend the array aperture. The DOA estimation performance under single-frequency and multifrequency scenarios is compared. As shown in Fig. 5, the incorporation of multifrequency information significantly enhances the spatial aperture and DOF of the array, resulting in improved accuracy and superior performance in DOA estimation.

Then, a performance comparison is conducted under varying SNR and snapshot numbers. First, with the snapshot number fixed at 100, five signals uniformly distributed from -30° to 30° illuminate a ULA. The SNR varies from -10 to 20 dB to evaluate the DOA estimation performance using: 1) multifrequency information with two-element extrapolation; 2) multifrequency information with four-element extrapolation; and 3) conventional single-frequency arrays, as shown in Fig. 6(a). Subsequently, with the SNR fixed at 5 dB, the snapshot number increases from 100 to 1000 to analyze the DOA estimation performance versus snapshot number, as presented in Fig. 6(b).

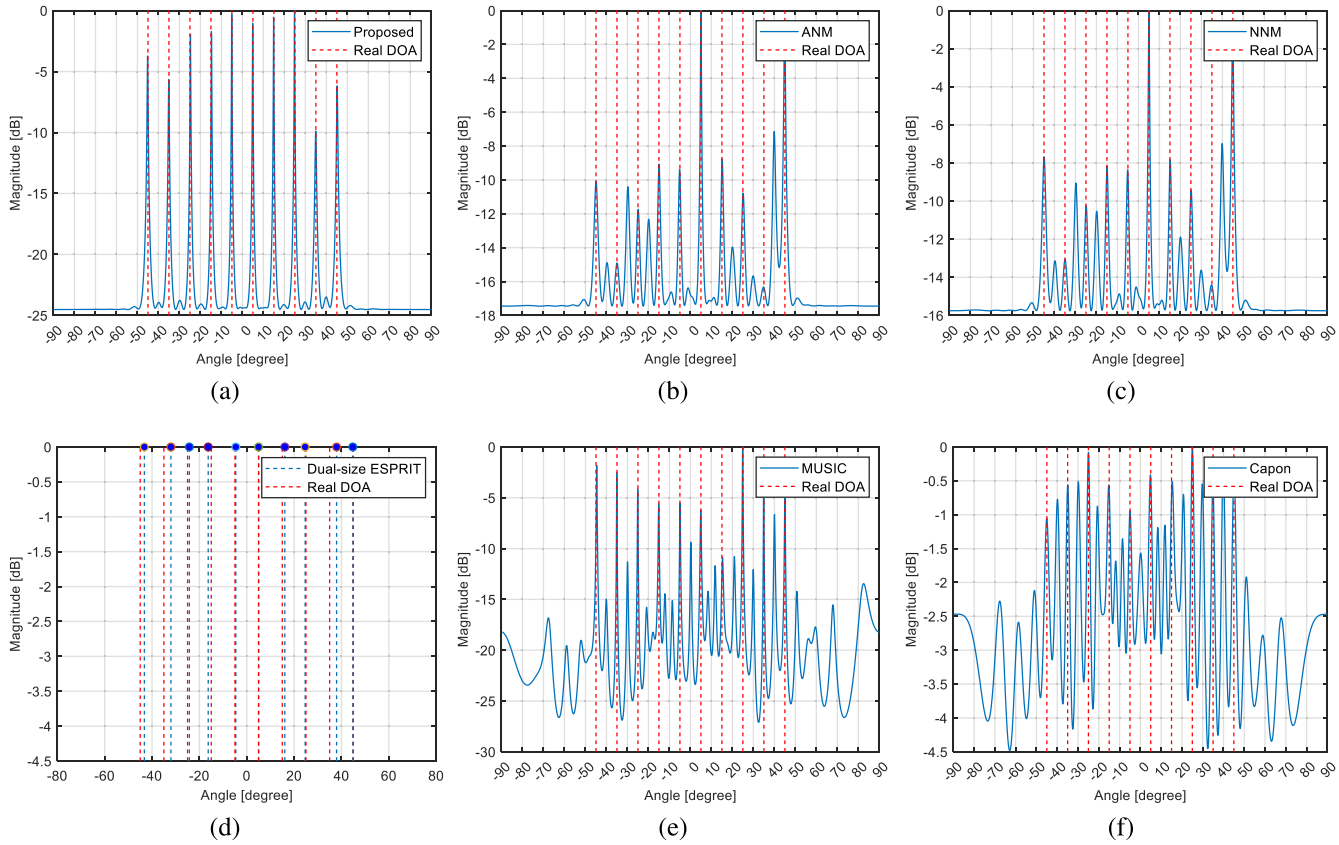

Fig. 7. Performance comparison of different algorithms. (a) Proposed method. (b) ANM. (c) NNM. (d) Dual-size ESPRIT. (e) MUSIC. (f) Capon.

TABLE I
RMSE COMPARISON OF DIFFERENT ALGORITHMS

Algorithm	The-proposed	ANM	NNM	Dual-size ESPRIT	MUSIC	Capon
RMSE (°)	0.14	2.25	2.29	1.72	8.37	8.37

The results demonstrate that the proposed multifrequency array consistently outperforms the traditional single-frequency array across a wide range of SNRs and snapshot numbers. Moreover, the DOA estimation accuracy improves with increasing numbers of extrapolated array elements, confirming the effectiveness of the proposed method in enhancing estimation precision.

C. Multiple Signal Doa Estimation

We subsequently compare the DOA estimation performance of different algorithms. Under the conditions of SNR = 0 dB and $T = 400$, eleven targets uniformly distributed from $-45°$ to $45°$ impinge on the distributed array as shown in Fig. 1. The estimation results of the proposed method are compared with the NNM DOA estimation method, the ANM DOA estimation method, the dual-size ESPRIT algorithm, the conventional MUSIC algorithm, and the Capon algorithm without array interpolation, as illustrated in Fig. 7.

It can be seen that the dual-size ESPRIT algorithm with array interpolation and baseline ambiguity resolution can estimate multiple targets with reasonable accuracy. However, its estimation precision degrades when the number of targets increases, manifesting as angular deviations for certain targets. In contrast, the proposed method effectively enhances DOA estimation accuracy by exploiting multifrequency information and employing a more precise rank approximation, thereby completing the array aperture more effectively. However, the conventional MUSIC and Capon algorithms without array interpolation suffer from significant spurious peaks and exhibit substantial angular estimation errors, making them inadequate for precise multitarget resolution requirements. In addition, to make the comparison clearer, Table I shows the quantitative RMSE results of different algorithms under typical SNR and snapshot conditions based on Fig. 7.

D. Performance Comparison of Different Algorithms

This section evaluates the RMSE performance of various algorithms under different SNRs and snapshot numbers, with 200 Monte Carlo trials conducted for statistical reliability.

Eleven targets distributed from $-55°$ to $45°$ impinging on the distributed array shown in Fig. 1. Fig. 8 presents the RMSE versus SNR performance with snapshots fixed at 200, where the SNR varies from -15 to 20 dB. The results demonstrate that the proposed algorithm achieves the lowest RMSE across the larger SNR range, indicating its superior DOA estimation capability. Similarly, Fig. 9 demonstrates the RMSE performance with snapshot numbers increasing from 100 to 1000 under a constant 5-dB SNR condition. The proposed method consistently outperforms other distributed

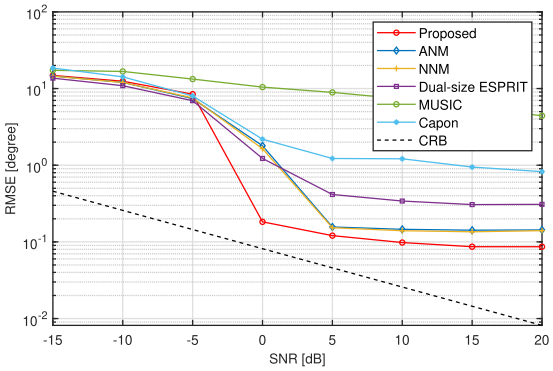

Fig. 8. RMSEs of estimated DOAs versus SNR.

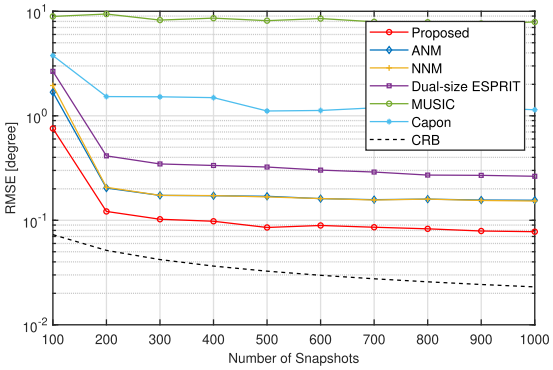

Fig. 9. RMSEs of estimated DOAs versus number of snapshots.

array DOA estimation algorithms by maintaining lower RMSE values, thereby validating its effectiveness.

To further validate the effectiveness of the proposed joint multifrequency extrapolation and low-rank matrix completion method, three cases are considered as follows.

Case I: The proposed method.
Case II: DOA estimation using low-rank matrix reconstruction under a single-frequency condition.
Case III: DOA estimation directly based on the original single-frequency array covariance matrix.

Each scenario was evaluated over 200 Monte Carlo trials. The RMSE performance is first evaluated with the snapshot number fixed at 100 while varying the SNR from -15 to 20 dB. Subsequently, with the SNR fixed at 0 dB, the snapshot number is varied from 100 to 1000 to evaluate the corresponding RMSE performance, as illustrated in Fig. 10.

The results indicate that, under low SNR or limited snapshots, low-rank reconstruction alone can partially improve performance, but there remains a significant gap compared to the joint method leveraging multifrequency information. The latter maintains optimal performance under a wider range of conditions, fully demonstrating the synergistic advantage of combining multifrequency extrapolation with low-rank reconstruction. The proposed method provides a cooperative aperture extension effect in distributed array DOA estimation, effectively mitigating spectral ambiguity caused by sparse spatial sampling and improving both resolution and estimation robustness.

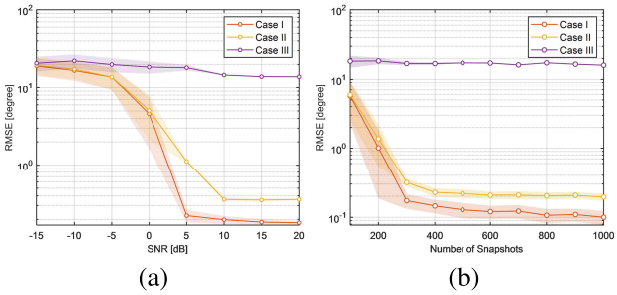

Fig. 10. Performance comparison of different cases. (a) RMSEs of estimated DOAs versus SNR. (b) RMSEs of estimated DOAs versus number of snapshots.

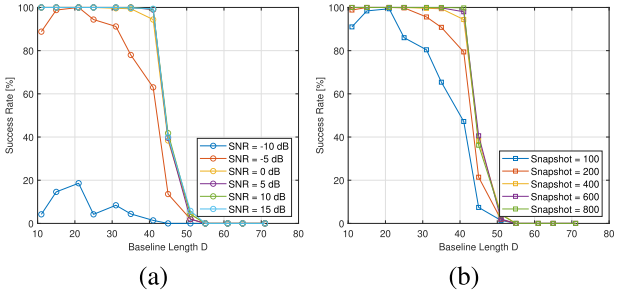

Fig. 11. Success rates versus baseline. (a) Success rates under different SNR. (b) Success rates under different snapshot numbers.

E. Evaluation of the Proposed Algorithm Across Different Array Baseline Lengths

To further evaluate the robustness and ambiguity-resolution capability of the proposed algorithm under different baseline configurations, we conduct an extensive set of simulations. These experiments analyze their DOA estimation performance across a range of baseline lengths, SNR levels, and snapshot numbers, with particular emphasis on the success rate of multitarget direction estimation under various array settings.

In particular, under the same distributed nested subarray configuration with $N_1 = N_2 = 3$, the baseline lengths were set as $D = [11, 21, 31, 41, 51, 61, 71]$. When the number of snapshots was fixed at 400, the SNR values were set to $[-10, -5, 0, 5, 10, 15]$ dB, and the incident angles were from $\theta = [45°, 40°, 30°, 10.8°, 0°, -10°]$. A DOA estimate was considered successful if its deviation from the true angle was less than 1°. Each experiment was repeated 200 times using Monte Carlo simulations to calculate the success estimation rate. Furthermore, with SNR fixed at 0 dB, we evaluated the success rates under different snapshot numbers from 100 to 800, as shown in Fig. 11.

The results demonstrate that under moderate-to-high SNR conditions (SNR > -5 dB) and sufficient snapshots (more than 400), the proposed algorithm maintains a high success rate even as the baseline length increases. However, when the baseline length exceeds 40, the success rate begins to decline, and it drops to zero as the baseline increases further. Under low SNR or limited-snapshot conditions, the overall estimation performance degrades accordingly. These findings indicate that the proposed algorithm exhibits a certain performance threshold for ambiguity-free estimation in distributed

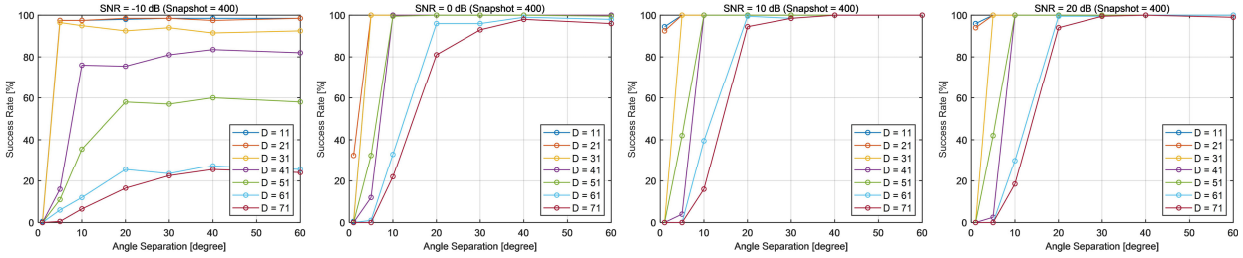

Fig. 12. Success rates versus angle separation. (a) SNR = −10 dB. (b) SNR = 0 dB. (c) SNR = 10 dB. (d) SNR = 20 dB.

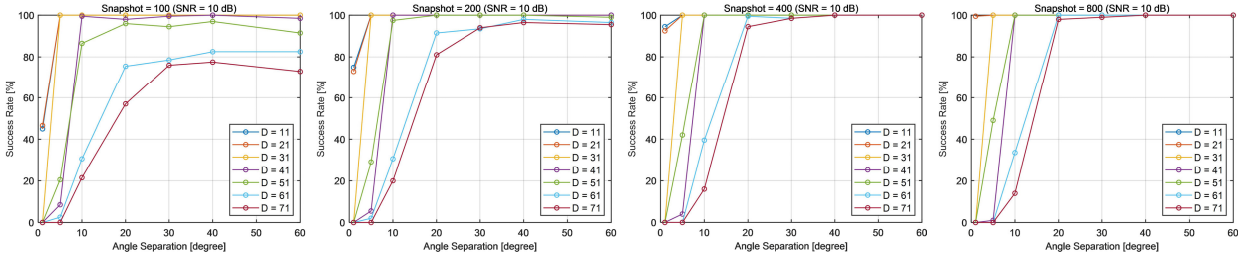

Fig. 13. Success rates versus angle separation. (a) Snapshot = 100. (b) Snapshot = 200. (c) Snapshot = 400. (d) Snapshot = 800.

arrays, yet remains robust within the feasible baseline range. Moreover, within reasonable SNR and snapshot conditions, the success rate of the proposed method consistently remains high.

We further conduct a series of experiments to evaluate the performance of the proposed algorithm under different baseline lengths and angle separations, thereby assessing its robustness limits and ambiguity-resolving capability. In particular, two groups of experiments were conducted to comprehensively evaluate the algorithm's performance. In the first group, the snapshot number was fixed at 400, and the success rate was evaluated under SNRs of −10, 0, 10, and 20 dB as the angle separation varied. In the second group, the SNR was fixed at 10 dB, and the success rate was evaluated as the angle separation varied for snapshot numbers of 100, 200, 400, and 800. To investigate the influence of baseline length, both experiments were performed under various baseline configurations $D = [11, 21, 31, 41, 51, 61, 71]$. Three sources arriving from distinct directions were considered, where one source was fixed at $-15°$, and the angular separations between the other two sources were set to $\Delta\theta = [1°, 5°, 10°, 20°, 30°, 40°, 60°]$. Each experimental condition was evaluated using 200 Monte Carlo simulations, and an estimation was considered successful when all angle estimation errors were within 1°. The results are presented in Figs. 12 and 13.

Experimental results demonstrate that when the baseline is short, the proposed algorithm achieves high resolution and a high success rate even at small angle separations, showing strong anti-ambiguity capability. As the baseline length increases, the array becomes more sensitive to small angular separations, leading to degraded estimation performance when the sources are closely spaced. As the baseline length exceeds around 51, the algorithm requires larger angular separations to correctly resolve ambiguities, yet it still performs well for source pairs with sufficiently large separations.

F. Computational Complexity Analysis

The computational complexity of the proposed method mainly arises from three stages: the estimation and extrapolation of multifrequency covariance matrices, the solution of the low-rank matrix completion model based on the Schatten-p norm, and the subsequent DOA estimation using the MUSIC algorithm. In the multifrequency covariance estimation stage, a sample covariance matrix of size $N \times N$ needs to be computed for each operating frequency point. For T snapshots and Q extrapolated frequency points, the total computational complexity is $\mathcal{O}(QTN^2)$. In the subsequent low-rank matrix completion using the IRLS algorithm, the dominant cost per iteration arises from solving a Sylvester equation, giving a complexity of $\mathcal{O}(P^3)$, and hence the overall complexity for this step is $\mathcal{O}(N_{\max}P^3)$. For the MUSIC algorithm, the main cost comes from eigenvalue decomposition and spectral search over Q_s grid points, with complexity $\mathcal{O}(P^3 + P^2Q_s)$. Therefore, the overall computational complexity of the proposed method is $\mathcal{O}(QTN^2) + \mathcal{O}(N_{\max}P^3) + \mathcal{O}(P^3 + P^2Q_s)$.

For the ANM and NNM algorithms, the computational complexity is mainly dominated by the low-rank matrix reconstruction formulated as a semidefinite programming (SDP) problem and the subsequent DOA estimation using the MUSIC algorithm. Both methods employ the CVX toolbox in MATLAB to solve the SDP, where each iteration requires approximately $\mathcal{O}(P^3)$ operations. The total number of iterations is proportional to $\mathcal{O}(\sqrt{P}\log(1/\varepsilon))$, where ε represents the solution accuracy. Hence, the overall computational complexity of the ANM and NNM algorithms can be expressed as $\mathcal{O}(TN^2) + \mathcal{O}(P^{3.5}) + \mathcal{O}(P^3 + P^2Q_s)$.

TABLE II
COMPUTATIONAL COMPLEXITIES OF DIFFERENT ALGORITHMS

Algorithms	Computational complexity
The proposed	$\mathcal{O}\left(QTN^2\right)+\mathcal{O}\left(N_{max}P^3\right)+\mathcal{O}\left(P^3+P^2Q_s\right)$
ANM	$\mathcal{O}\left(TN^2\right)+\mathcal{O}\left(P^{3.5}\right)+\mathcal{O}\left(P^3+P^2Q_s\right)$
NNM	$\mathcal{O}\left(TN^2\right)+\mathcal{O}\left(P^{3.5}\right)+\mathcal{O}\left(P^3+P^2Q_s\right)$
MUSIC	$\mathcal{O}\left(P^3+P^2Q_s\right)$
Capon	$\mathcal{O}\left(P^3+P^2Q_s\right)$
Dual-size ESPRIT	$\mathcal{O}\left(M_1^2T+M_2^2T+M_1^3+M_2^3\right)$

Fig. 14. Physical verification setup.

The computational complexity of the MUSIC and Capon algorithms mainly arises from eigenvalue decomposition and matrix inversion, respectively, yielding an overall complexity of $\mathcal{O}(P^3 + P^2Q_s)$. For the dual-size ESPRIT algorithm, two subarrays with different scales are employed to obtain additional DOF. Its computational complexity mainly comes from covariance estimation and eigenvalue decomposition for both subarrays. Let M_1 and M_2 denote the number of elements in the two subarrays. The corresponding complexity is $\mathcal{O}(M_1^2T + M_2^2T + M_1^3 + M_2^3)$.

The computational complexities of different algorithms are presented in Table II. Compared with convex optimization-based algorithms, the proposed method exhibits lower computational complexity and demonstrates a clear efficiency advantage when dealing with large-scale array scenarios.

G. Performance Analysis Based on Experimental Data

The proposed method was validated using data collected from a passive radar system employing a 12-element ULA as the receiving antenna. The system captures moving target echoes while contending with direct signals from the primary base station and co-channel interference. All received signals undergo digital signal processing for subsequent analysis. The base station, located at approximately 0° with a range of 200 m, serves as the illuminator of opportunity in the experimental scenario as shown in Fig. 14.

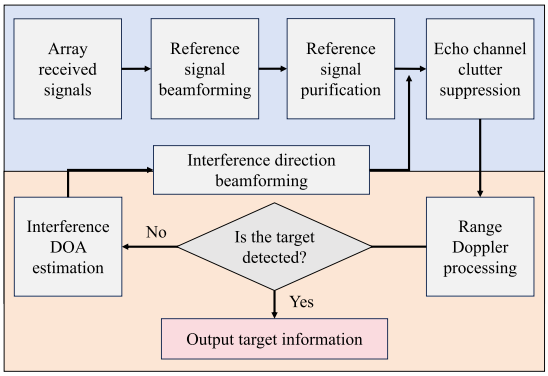

Fig. 15. Experimental procedure.

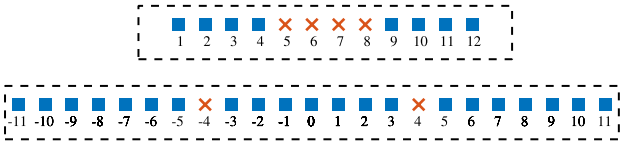

Fig. 16. Physical sensor array and its virtual counterpart.

The proposed method combines multifrequency information with a low-rank matrix completion model for DOA estimation. In this experiment, LTE signals at 2.1-GHz carrier frequency were utilized as opportunistic illumination sources to detect both direct-path and multipath interference from the base station. This enables reference signal beamforming and interference suppression, thereby facilitating subsequent moving target detection. The experimental workflow is illustrated in Fig. 15.

For distributed array validation, a sparse array configuration was created by selecting elements 1–4 and 9–12 from the original ULA. The equivalent receiving array configuration is illustrated in Fig. 16. Due to the high center frequency and limited bandwidth of the signals, multifrequency array extrapolation was not employed, and validation proceeded directly using the low-rank matrix completion algorithm.

The signal processing pipeline initiates with directional beamforming of the multichannel echoes toward the reference signal direction to isolate the direct-path component from the base station. After performing clutter suppression using the reference signal, range-Doppler processing reveals residual co-channel interference in near-range cells and distinct bright streaks near zero-Doppler bins, indicating the presence of multidirectional interference that would compromise target detection. To address this, we construct a virtual extended aperture using selected sparse array elements and apply the proposed low-rank matrix completion model to reconstruct the missing aperture data. The reconstructed array data then undergoes MUSIC-based DOA estimation, where spectral peak identification determines interference directions for subsequent null-steering beamforming and clutter suppression in range-Doppler processing. Fig. 17 demonstrates the comparative results, where the proposed method shows superior DOA estimation accuracy and interference suppression capability

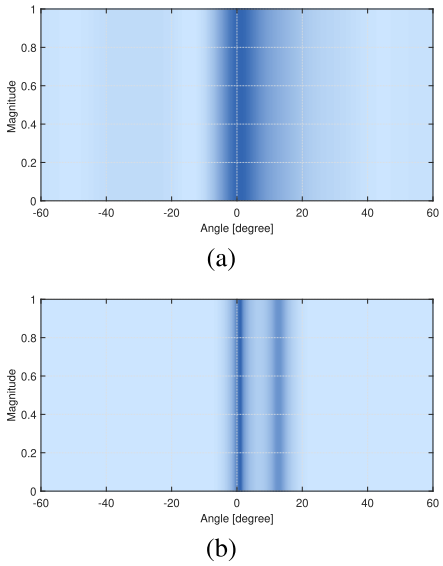

Fig. 17. Spatial spectrum estimation. (a) MUSIC. (b) Proposed.

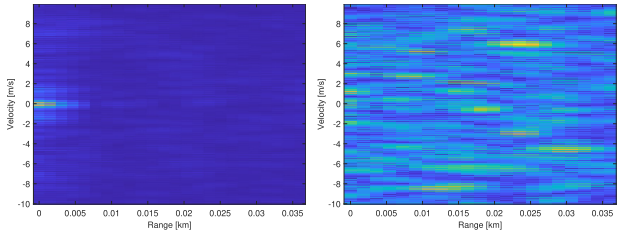

Fig. 18. Range-Doppler diagram. (a) Before suppression. (b) After suppression.

compared to conventional ULA configurations. In particular, as shown in Fig. 18, the accurate DOA estimation enables effective suppression of high-power interference, as evidenced by the significantly reduced energy in near-range cells on the RD map. This improvement verifies the effectiveness of the proposed low-rank completion model in enhancing distributed array performance for practical passive radar applications.

Experimental results demonstrate that the proposed algorithm effectively extracts spatial spectral information from both the base station and its multipath signals, thereby providing substantial support for subsequent target detection.

V. Conclusion

This article presents a high-precision, ambiguity-free DOA estimation framework based on a distributed sparse array architecture. Under constrained hardware resources and multitarget scenarios, conventional ULAs often exhibit performance limitations that fail to satisfy the requirements of modern direction-finding systems. In contrast, distributed sparse arrays achieve enhanced DOF through optimized spatial configuration, while inevitably introducing challenging ambiguity problems in parameter estimation.

To address this, we develop a novel DOA estimation method that integrates multifrequency information fusion and low-rank matrix reconstruction. In particular, nested array configurations are employed to expand the equivalent aperture of subarrays, thereby fully exploiting the DOF provided by sparsity. The frequency diversity characteristics are utilized to compensate for array aperture discontinuities at the virtual element level, thereby effectively suppressing grating lobes induced by extended baseline configurations. Furthermore, the Schatten-p norm is employed to characterize the low-rank structure of the received signal matrix, enabling the formulation of a low-rank matrix completion model. The missing data across subarrays is efficiently reconstructed using the IRLS algorithm, enabling accurate subspace-based DOA estimation while reducing computational complexity.

Extensive simulation and experimental results demonstrate that the proposed method achieves superior estimation accuracy and robustness in complex electromagnetic environments and multitarget scenarios, especially under low SNR conditions and with limited snapshots.

In addition, the method significantly extends the virtual aperture of the array, providing a practical and effective solution for deploying distributed arrays in applications such as target localization and integrated sensing and communication. Future research will investigate the robustness of the proposed method under scenarios involving coherent sources and array imperfections, aiming to enhance the robustness and practical applicability of the proposed framework.

References

[1] R. C. Heimiller, J. E. Belyea, and P. G. Tomlinson, "Distributed array radar," *IEEE Trans. Aerosp. Electron. Syst.*, vol. AES-19, no. 6, pp. 831–839, Nov. 1983.

[2] M. Pan et al., "Efficient joint DOA and TOA estimation for indoor positioning with 5G picocell base stations," *IEEE Trans. Instrum. Meas.*, vol. 71, pp. 1–19, 2022.

[3] M. R. Shamsian, M. Sadeghi, and F. Behnia, "Joint TDOA and DOA single site localization in NLOS environment using virtual stations," *IEEE Trans. Instrum. Meas.*, vol. 73, pp. 1–10, 2024.

[4] H. Chen, W. Wang, W. Liu, Y. Tian, and G. Wang, "An exact near-field model based localization for bistatic MIMO radar with COLD arrays," *IEEE Trans. Veh. Technol.*, vol. 72, no. 12, pp. 16021–16030, Dec. 2023.

[5] R. Schmidt, "Multiple emitter location and signal parameter estimation," *IEEE Trans. Antennas Propag.*, vol. AP-34, no. 3, pp. 276–280, Mar. 1986.

[6] Z. Yang, "Nonasymptotic performance analysis of ESPRIT and spatial-smoothing ESPRIT," *IEEE Trans. Inf. Theory*, vol. 69, no. 1, pp. 666–681, Jan. 2023.

[7] A. Kiyaei, W. Ahmad, S. Zakir, E. M. Al Seragi, A. H. Shah, and S. Zeinolabedinzadeh, "Interference-tolerant wireless distributed beamforming receiver array with low-latency frequency synchronization," *IEEE Trans. Microw. Theory Techn.*, vol. 73, no. 7, pp. 3893–3906, Jul. 2025.

[8] P. Chen, Z. Chen, B. Zheng, and X. Wang, "Efficient DOA estimation method for reconfigurable intelligent surfaces aided UAV swarm," *IEEE Trans. Signal Process.*, vol. 70, pp. 743–755, 2022.

[9] B. Li, B. Xu, and Y. Yuan, "Preestimation-based array interpolation approach to coherent source localization using multiple sparse subarrays," *IEEE Signal Process. Lett.*, vol. 16, no. 2, pp. 81–84, Feb. 2009.

[10] J.-H. Lee and J.-M. Woo, "Interferometer direction-finding system with improved DF accuracy using two different array configurations," *IEEE Antennas Wireless Propag. Lett.*, vol. 14, pp. 719–722, 2015.

[11] H. Gazzah and K. Abed-Meraim, "Optimum ambiguity-free isotropic antenna arrays," in *Proc. IEEE Int. Conf. Acoust., Speech Signal Process.*, Apr. 2009, pp. 2157–2160.

[12] K. T. Wong and M. D. Zoltowski, "Direction-finding with sparse rectangular dual-size spatial invariance array," *IEEE Trans. Aerosp. Electron. Syst.*, vol. 34, no. 4, pp. 1320–1336, Aug. 1998.

[13] S. Miron, Y. Song, D. Brie, and K. T. Wong, "Multilinear direction finding for sensor-array with multiple scales of invariance," *IEEE Trans. Aerosp. Electron. Syst.*, vol. 51, no. 3, pp. 2057–2070, Jul. 2015.

[14] T. Long, H. Zhang, T. Zeng, Q. Liu, X. Chen, and L. Zheng, "High accuracy unambiguous angle estimation using multi-scale combination in distributed coherent aperture radar," *IET Radar, Sonar Navig.*, vol. 11, no. 7, pp. 1090–1098, May 2017.

[15] A. Moffet, "Minimum-redundancy linear arrays," *IEEE Trans. Antennas Propag.*, vol. AP-16, no. 2, pp. 172–175, Mar. 1968.

[16] P.-C. Huang and C.-L. Liu, "Coarray-based pattern synthesis for minimum hole arrays," in *Proc. Int. Symp. Antennas Propag. (ISAP)*, Jan. 2021, pp. 443–444.

[17] P. Pal and P. P. Vaidyanathan, "Nested arrays: A novel approach to array processing with enhanced degrees of freedom," *IEEE Trans. Signal Process.*, vol. 58, no. 8, pp. 4167–4181, Aug. 2010.

[18] Y. Su, X. Wang, and X. Lan, "Co-prime array interpolation for DOA estimation using deep matrix iterative network," *IEEE Trans. Instrum. Meas.*, vol. 73, pp. 1–12, 2024.

[19] Z. Yang, S. Ma, Y. Liu, H. Zhang, and X. Lyu, "DOA estimation for enhanced coprime planar arrays via low-rank matrix completion and sparse regularization," *Appl. Acoust.*, vol. 239, pp. 110824–110835, Nov. 2025.

[20] Z. Zheng, Y. Huang, W.-Q. Wang, and H. C. So, "Direction-of-arrival estimation of coherent signals via coprime array interpolation," *IEEE Signal Process. Lett.*, vol. 27, pp. 585–589, 2020.

[21] S. Gao, H. Ma, H. Liu, and Y. Yang, "DOD and DOA estimation from incomplete data based on PARAFAC and atomic norm minimization method," *IEEE Trans. Geosci. Remote Sens.*, vol. 61, 2023, Art. no. 5100314.

[22] S. K. Yadav and N. V. George, "Fast direction-of-arrival estimation via coarray interpolation based on truncated nuclear norm regularization," *IEEE Trans. Circuits Syst. II, Exp. Briefs*, vol. 68, no. 4, pp. 1522–1526, Apr. 2021.

[23] Z. Yang, S. Ma, Y. Liu, H. Zhang, and X. Lyu, "DOA estimation of coherent sources via low-rank matrix decomposition," *IEEE Wireless Commun. Lett.*, vol. 13, no. 11, pp. 3049–3053, Nov. 2024.

[24] E. BouDaher, Y. Jia, F. Ahmad, and M. G. Amin, "Multi-frequency co-prime arrays for high-resolution direction-of-arrival estimation," *IEEE Trans. Signal Process.*, vol. 63, no. 14, pp. 3797–3808, Jul. 2015.

[25] M. Guo, Y. D. Zhang, and T. Chen, "Performance analysis for uniform linear arrays exploiting two coprime frequencies," *IEEE Signal Process. Lett.*, vol. 25, no. 6, pp. 838–842, Jun. 2018.

[26] S. Zhang, A. Ahmed, Y. D. Zhang, and S. Sun, "DOA estimation exploiting interpolated multi-frequency sparse array," in *Proc. IEEE 11th Sensor Array Multichannel Signal Process. Workshop (SAM)*, Jun. 2020, pp. 1–5.

[27] S. Zhang, A. Ahmed, Y. D. Zhang, and S. Sun, "Enhanced DOA estimation exploiting multi-frequency sparse array," *IEEE Trans. Signal Process.*, vol. 69, pp. 5935–5946, 2021.

[28] Y. Park, P. Gerstoft, Y. Wu, and M. B. Wakin, "Atomic norm denoising for multi-frequency-snapshot doa estimation," in *Proc. IEEE 13rd Sensor Array Multichannel Signal Process. Workshop (SAM)*, Jul. 2024, pp. 1–5.

[29] J. Wen, J. Yi, X. Wan, Z. Gong, and J. Shen, "DOA estimation based on multi-frequency joint sparse Bayesian learning for passive radar," *J. Syst. Eng. Electron.*, vol. 33, no. 5, pp. 1052–1063, Oct. 2022.

[30] Y. Wu, M. B. Wakin, and P. Gerstoft, "Gridless DOA estimation under the multi-frequency model," in *Proc. IEEE Int. Conf. Acoust., Speech Signal Process. (ICASSP)*, May 2022, pp. 5982–5986.

[31] Z. Guo and W. Dai, "Joint multi-band DOA estimation using low-rank matrix recovery," in *Proc. IEEE Int. Conf. Acoust., Speech Signal Process. (ICASSP)*, Apr. 2024, pp. 8466–8470.

[32] J. Cheng, K. Guan, and F. Quitin, "Direction-of-arrival estimation with virtual antenna array: Observability analysis, local oscillator frequency offset compensation, and experimental results," *IEEE Trans. Instrum. Meas.*, vol. 70, pp. 1–13, 2021.

[33] Q. Guo, Z. Xin, T. Zhou, and S. Xu, "Off-grid space alternating sparse Bayesian learning," *IEEE Trans. Instrum. Meas.*, vol. 72, pp. 1–10, 2023.

[34] C. Lu, Z. Lin, and S. Yan, "Smoothed low rank and sparse matrix recovery by iteratively reweighted least squares minimization," *IEEE Trans. Image Process.*, vol. 24, no. 2, pp. 646–654, Feb. 2015.